Macromolecules
ARTICLE

Macromolecules **2010**, *43*, 9049–9055 **9049**
DOI: 10.1021/ma100959v

Investigation of True Surface Morphology and Nanomechanical Properties of Poly(styrene-*b*-ethylene-*co*-butylene-*b*-styrene) Using Nanomechanical Mapping: Effects of Composition

Dong Wang,* So Fujinami, Hao Liu, Ken Nakajima, and Toshio Nishi

WPI Advanced Institute for Materials Research, Tohoku University, 2-1-1 Katahira, Aoba, Sendai 980-8577, Japan

Received April 30, 2010; Revised Manuscript Received August 29, 2010

ABSTRACT: The surface morphology and nanomechanical properties of poly(styrene-*b*-ethylene-*co*-butylene-*b*-styrene) (SEBS) having different compositions were investigated using nanomechanical mapping measurements based on atomic force microscopy. We obtained the deformation image, true surface morphology, high-resolution Young's modulus map, and map of deviated work simultaneously in a force mapping. Such maps were successfully used to identify and characterize the composition and better understand the relationship between microstructure and properties of SEBS samples. It is found that the obtained Young's modulus and deformation values, both for polystyrene (PS) or poly(ethylene-*co*-butylene) (PEB) blocks, strongly depend on the microstructure that is dominated by the composition. As the PS composition increase, the modulus of PS blocks increases from 19.2 ± 2.5 MPa for SEBS (10/80/10) to 823.0 ± 168.1 MPa for SEBS (33.5/33/33.5), while PEB's increases from 8.7 ± 2.1 MPa for SEBS (10/80/10) to 97.6 ± 17.8 MPa for SEBS (33.5/33/33.5). The calculated map of deviated work from elastic model will be a convenient technique to visualize the distribution of viscoelasticity. Furthermore, the reconstructed true height image reveals the true topographic feature free from sample deformation.

1. Introduction

An important class of thermoplastic elastomers (TPE) includes block copolymers that are covalently joined homopolymer chains. These materials are known to self-assemble into a variety of ordered structures such as spheres, cylinders, and lamellae at nanometer scales, by a process called microphase separation. The latter is a consequence of the intramolecular phase separation between homopolymer chains. Through variation of composition, processing conditions, and molecular weight, dimensions, nature and orientation of the block copolymer nanostructures can be controlled.[1−3]

Owing to the widely separated glass transition temperature T_g of the constituent phases, poly(styrene-*b*-polybutadiene-*b*-styrene) (SBS) and poly(styrene-*b*-ethylene-*co*-butylene-*b*-styrene) (SEBS) triblock copolymers provide a broad range of physical properties. The hard polystyrene (PS) blocks form domains that serve as filler and as physical cross-links to connect the elastomeric soft polybutadiene (PB) or poly(ethylene-*co*-butylene) (PEB) blocks.[2,3] Owing to the increased interest in versatile ordered structures (spheres, cylinders, and lamellae, etc.) and outstanding mechanical (stiffness, strength, toughness, etc.) properties of these block copolymers, a better understanding of their mechanical properties at the nanoscale and a deeper insight into the microstructure−property correlation is required. To date, most of the studies on structures of these materials have been done using small-angle X-ray scattering (SAXS), electron and scanning force microscopy, including in situ microscopy.[4−6] However, neither SAXS nor electron microscopy techniques can be used to determine mechanical information or directly link the mechanical properties to the structures of the materials.

Recently developed atomic force microscopy (AFM) nanomechanical mapping techniques such as AFM tapping mode using torsional harmonic cantilevers,[7,8] band excitation method,[9] contact resonance based technique,[10,11] and a commonly used technique, force volume mode (FV),[6,12−14] are simple and efficient methods to obtain the mechanical properties of materials with surface heterogeneity. Attempts have been made to utilize those techniques to map the nanomechanical properties of some block copolymers and supermolecular self-assembled systems.[15−19] In a previous communication,[6] we reported a nanomechanical mapping technique that is based on a combination of Johnson−Kendall−Robert (JKR)[20] contact mechanics and "two-point method"[21] to interpret AFM force measurements. With this technique, high-resolution maps of Young's modulus, deviated work from JKR theory, deformation image, and true surface topography can be obtained simultaneously in a force mapping.

In this paper, we present results from systematic studies aimed at characterizing the compositional effect on surface morphology and nanomechanical properties of poly(styrene-*b*-ethylene-*co*-butylene-*b*-styrene) (SEBS) triblock copolymers. Herein, we directly correlate the structures to changes in mechanical properties (Young's modulus), which will enable us to have a deeper insight into microstructure−property correlations.

2. Experimental Section

Four types of SEBS samples were supplied by Asahi KASEI Corp. and used without further treatment. The sample characteristics including component weight ratio, number-average molecular weight, M_n, and molecular weight distribution M_w/M_n are listed in Table 1. Film samples with thickness about 10 μm were prepared by solvent-casting a 0.004 g/mL SEBS toluene solution onto cleaned glass slides. Toluene is a nonselective solvent to both the PS and PEB block, but it is only a little better for PS block chains in solubilization than for PEB block chains.[22,23] The as-prepared films were first dried in a fume hood for 1 day and then

*To whom correspondence should be addressed. E-mail: wangdthu@wpi-aimr.tohoku.ac.jp.

Published on Web 10/07/2010

in vacuum at room temperature for another 3 days to remove residual solvent.

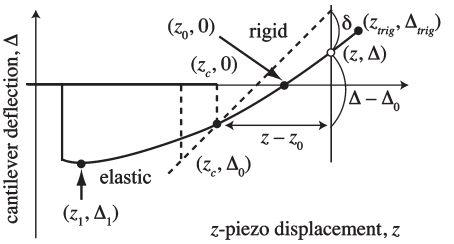

Figure 1. Schematic representation of the force−distance curves with an adhesive force between sample and AFM probe.

Table 1. SEBS Sample Characteristics

samples	component weight ratio	M_n	M_w/M_n
SEBS (10/80/10)	10/80/10	75 000	1.1
SEBS (14.5/71/14.5)	14.5/71/14.5	75 000	1.1
SEBS (21/58/21)	21/58/21	74 000	1.1
SEBS (33.5/33/33.5)	33.5/33/33.5	70 000	1.1

Nanomechanical measurements were taken using the force volume (FV) mode on a commercial AFM system (MultiMode with a NanoScope V controller) under ambient conditions. The samples were scanned at constant force using an *E* scanner (Veeco Instruments, 2.5 μm in *z* and 10 × 10 μm in *x* and *y*) and triangular Si_3N_4 cantilevers with nominal spring constant of 0.32 N/m (SNL-10, Veecoprobes). Force−distance curves were collected over randomly selected surfaces 1 μm × 1 μm in area at a resolution of 128 × 128 pixels. In order to eliminate the effect of substrate stiffness, the value of the trigger set point (3 nm) was far less than 1% of the film thickness. The obtained force curves were analyzed using JKR contact mechanics. According to this model, the Young's modulus *E* is expressed by the following equation:

$$E = \frac{3(1-\nu^2)}{4} \times \frac{1.27F_1}{\sqrt{R(\delta_0 - \delta_1)^3}} \quad (1)$$

where ν is Poisson's ratio, *R* is the radius of curvature of the tip, and δ is the sample deformation. F_1 is the maximum adhesive force proposed by Sun in the "two-point method".[21] Reference 6 shows detailed analysis procedures for calculating the *E*. Besides

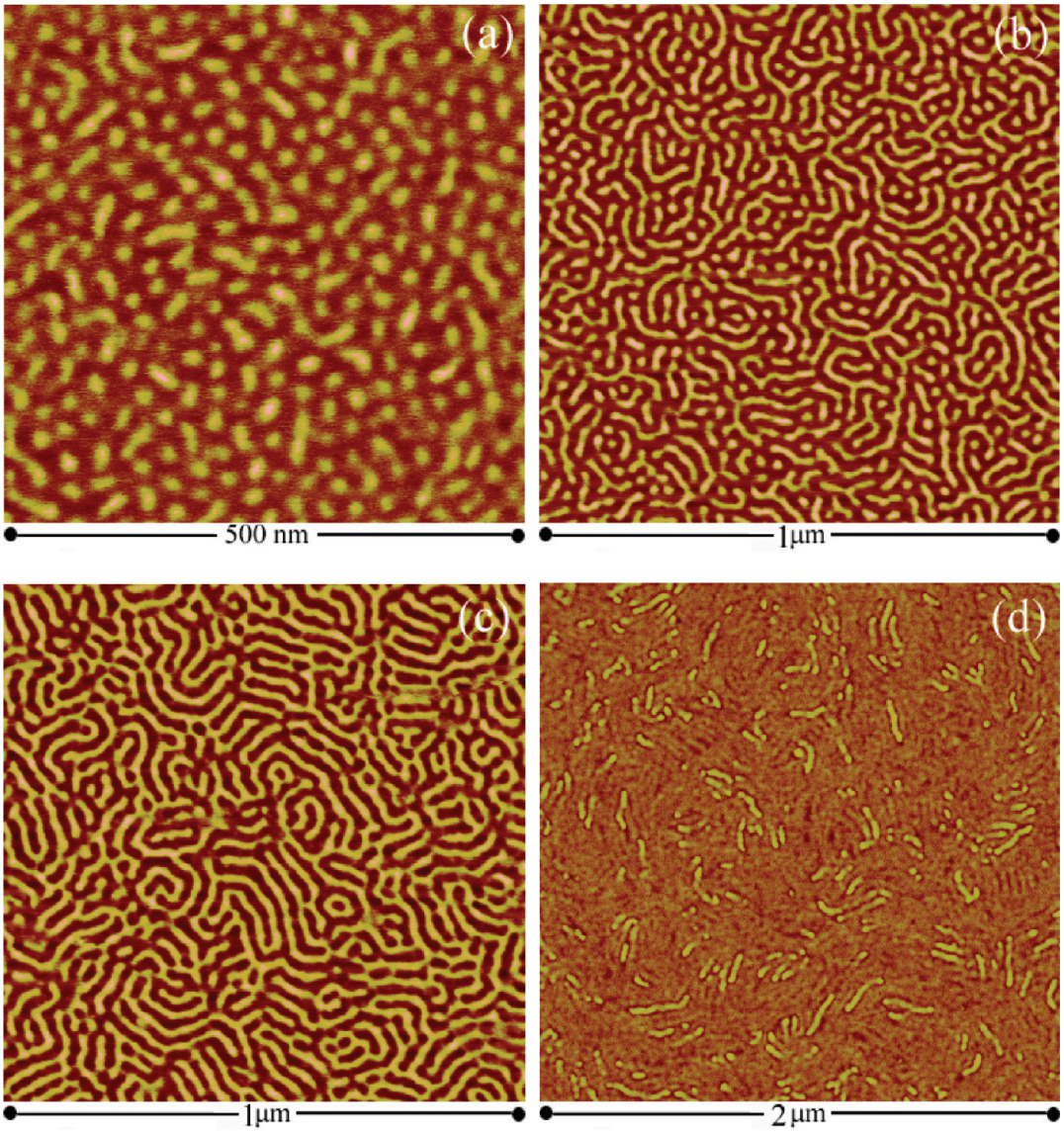

Figure 2. AFM tapping mode phase images of thin films of (a) SEBS (10/80/10), (b) SEBS (14.5/71/14.5), (c) SEBS (21/58/21), and (d) SEBS (33.5/33/33.5). Note the different scale in the images.

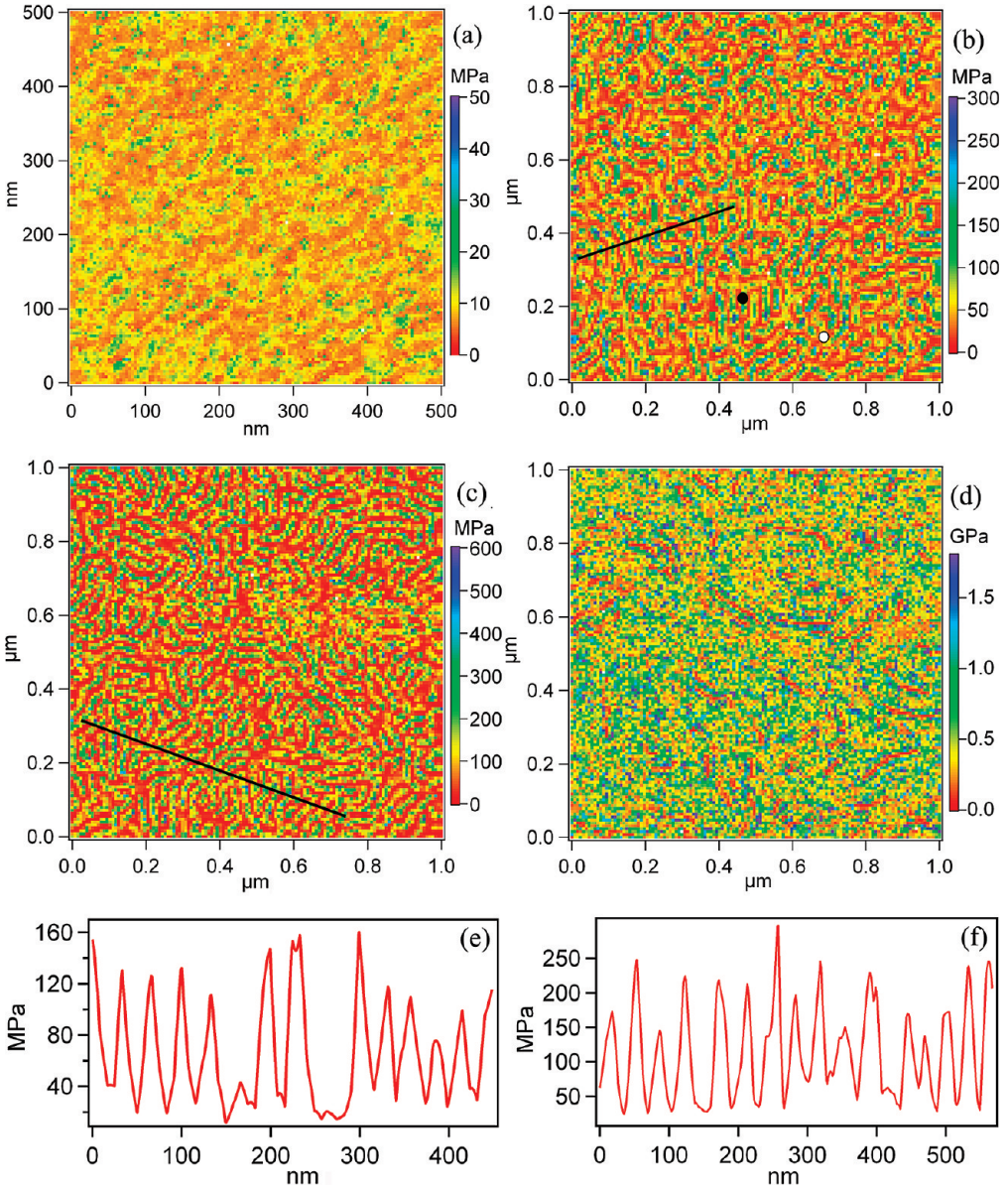

Figure 3. Young's modulus maps of (a) SEBS (10/80/10), (b) SEBS (14.5/71/14.5), (c) SEBS (21/58/21), and (d) SEBS (33.5/33/33.5). Note the different scale in the images. Numerical values across the sections indicated by the line in parts b and c are given in parts e and f, respectively.

mechanical properties, the apparent (original) height, deformation image, and true surface topography can be also obtained simultaneously. As schematically shown in Figure 1, a force−distance curve (the solid line is for compliant (soft) materials and the dashed line is for hard material as a reference) is a plot of the displacement, z of the piezoelectric scanner normal to the specimen's surface as the horizontal axis and the cantilever deflection, Δ as the vertical axis. In the force volume (FV) mode, the force−distance curves are recorded until a specified cantilever deflection value (trigger set-point), Δ_{trig}, is attained over a two-dimensional surface. At the same time, z-displacement values, z_{trig}, corresponding to the trigger set-point deflection are recorded to build the apparent height (topographic) image. Meanwhile, since we have a force−distance curve for each point, we can also estimate the maximum sample deformation value for each point, referring to eq 2.

$$\delta = (z_{trig} - z_c) - (\Delta_{trig} - \Delta_0) \quad (2)$$

where (z_c, Δ_0) is the contact point where the tip jump-in the sample surface because of the attractive forces. Then, two-dimensional arrays of sample deformation values can be regarded as the sample deformation image. We now have apparent height (z_{trig}) and sample deformation (δ) images taken at the same time and Δ_{trig} is the preset value and therefore constant for all of the force−distance curves. Then, the appropriate determination is performed for the contact point (the array of (z_c, Δ_0)), this realizes the reconstruction of the "true" surface topography, free from sample deformation.

For comparison, tapping mode data were also obtained with the same AFM and using a silicon cantilever with nominal spring constant of 20−80 N/m (MPP-11100, Veecoprobes). Moderate tapping forces corresponding to set-point ratios of ~0.70 were used.

3. Results and Discussion

The triblock copolymer SEBS consisting of hard and soft blocks that usually exhibit a phase-separated morphology has been widely studied by AFM techniques.[18,23−27] Figure 2 shows tapping mode phase image of SEBS samples having different component weight ratio. The characteristic phase-separated morphologies consisting of bright and dark nanophasic domains are observed. At low PS component (SEBS (10/80/10)), a coexistence of irregular short cylinders and spheres is generated. As the PS

weight ratio increases, the microstructure changes from a rod-like or an intermediate between the cylinder and lamellar structure for SEBS (14.5/71/14.5) to a well-ordered lamellar for SEBS (21/58/21). Further increase the PS weight ratio (SEBS (33.5/33/33.5) induces a great change in microstructure such that only the EB cylinder remains clearly visible. A possible reason may be attributed to the high PS weight ratio which increases the SEBS T_g a lot. The molecular mobility of PS decreases and it can not form well phase separated morphology during the experiment conditions. In such case, it is difficult to get clear PS features. It should be noted that such conclusions are drawn only from the results of the surface morphologies obtained by AFM tapping mode and the bulk morphologies of triblock copolymers mainly governed by the volume ratio of the phases. Here we only make this statement to compare the results obtained from AFM tapping mode with those of obtained from nanomechanical mapping measurements. In any case, the topography data alone provides little information about the chemical and mechanical heterogeneity of the SEBS films, which is especially apparent for Figure 2a−c. Without further analysis, identification of the bright or dark regions is not possible because some other researchers have assigned the bright regions to the hard PS component and dark regions to the soft rubbery PEB component.[18,24] In general, however, assigning chemical composition to the features observed in height and phase images is difficult unless additional experimentation is conducted.[28,29] Furthermore, the assignment of the bright or dark contrast to the hard or soft domain in phase imaging is not always straightforward. For example, several studies have assigned the brighter contrast to the stiffer material and the darker contrast to the softer material.[30−33] In other reports, the darker region has been attributed to the stiffer material and the lighter region to the softer material.[29,34] In order to provide an easy and efficient method for identifying the composition and investigating the mechanical properties of different regions, nanomechanical mapping measurements were performed.

Young's modulus maps obtained from nanomechanical mapping measurements for SEBS samples having different compositions are presented in Figure 3. As we observed, Young's modulus maps show a variety of ordered structures resembling the surface topography observed in the tapping mode (Figure 2). The characteristic phase-separated morphologies consisting of high and low Young's modulus regions are clearly exhibited. For the SEBS (10/80/10) sample, a coexistence of irregular short cylinders and spheres is observed from a Young's modulus map. As the PS weight ratio increases, the Young's modulus maps show well-ordered structure for the SEBS (14.5/71/14.5) and SEBS (21/58/21) samples. The Young's modulus map of the SEBS (33.5/33/33.5) is also very similar to the image obtained with AFM tapping mode. Moreover, this result further demonstrate that only the PEB block forms well ordered structure (the red areas with lower Young's modulus are considered to be the soft PEB blocks). The corresponding modulus profile across a section reveals the two chemical blocks have a large difference in modulus values (Figure 3, parts e and f). Therefore, such a map enables us to directly link the morphology and mechanical properties of the block copolymers. In the Young's modulus maps, the light green areas with higher Young's modulii are considered to be the hard PS blocks (in the case of Figure 3d, the PS blocks are not clear), while the red areas with lower Young's modulii are considered to be the soft PEB blocks. Two typical force−deformation curves corresponding to the two points indicated by white and dark circles in the Young's modulus image (Figure 3b) are shown in Figure 4. The curve fit using JKR contact mechanics is also superimposed in each case. The results show that JKR analysis of the withdrawing process fits well for the elastic PS component. However, deviations appear for the viscoelastic PEB component because of the viscoelastic effect. The Young's modulus calculated from force-deformation curves are presented in Table 2. Using the same evaluation method, we also investigated the Young's modulus of the bulk PS and PEB films (Table 2). It is found that as the PS weight ratio increases, the observed modulus of both the PEB and PS blocks dramatically increase. The Young's modulii of the PEB blocks of the SEBS (10/80/10) is about the same as the bulk value but much lower than SEBS (14.5/71/14.5), SEBS (21/58/21), and SEBS (33.5/33/33.5). Although the PS blocks for the SEBS (33.5/33/33.5) approaches the bulk value, it demonstrates a dramatic

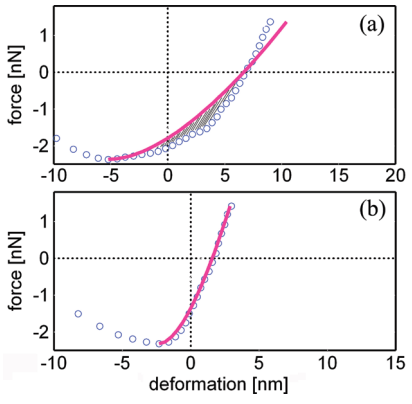

Figure 4. Force-deformation curves of local points indicated by the circles in Figure 3b. The curve-fitting against JKR contact was superimposed on each curve. (a) PEB region (white circle), (b) PS region (black circle). The shadow area in part a indicates the deviation from JKR theoretical curve.

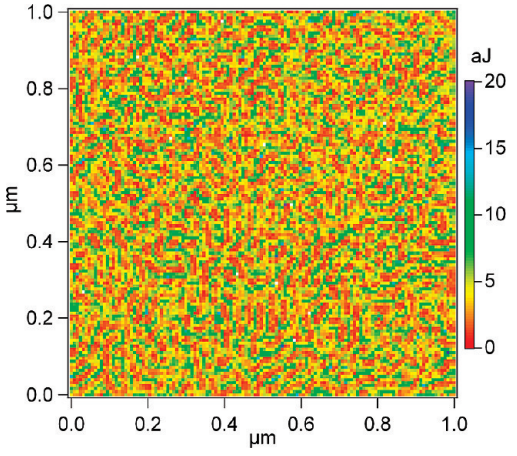

Figure 5. Map of deviated work of SEBS (14.5/71/14.5) sample from the JKR theory.

Table 2. Calculated Young's Modulus of the PS and PEB Blocks in SEBS Samples[a]

		samples			
		SEBS (10/80/10)	SEBS (14.5/71/14.5)	SEBS (21/58/21)	SEBS (33.5/33/33.5)
Young's modulus (MPa)	PS	19.2 ± 2.5	133.3 ± 26.0	209.0 ± 29.3	823.0 ± 168.1
	PEB	8.7 ± 2.1	25.6 ± 9.2	42.4 ± 16.9	97.6 ± 17.8

[a] The measured modulus value of pure PS and PEB is 2.02 ± 0.59 GPa and 10.1 ± 0.5 MPa, respectively.

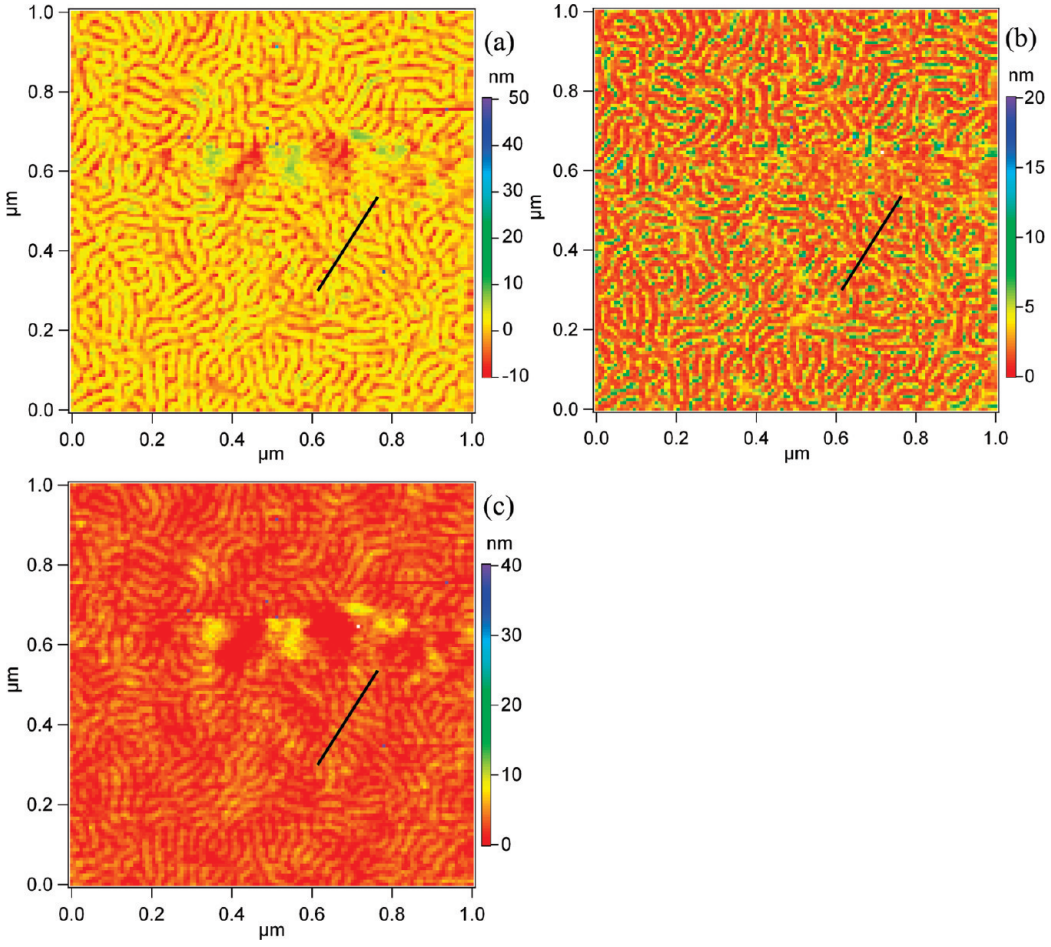

Figure 6. AFM topographic images of the SEBS (21/58/21) film. (a) original height, (b) deformation, and (c) reconstructed true height image.

decrease in stiffness for the other three SEBS samples. Previous work has shown that the hard substrate (usually, infinitely stiff solids as compared to compliant polymer layers) is a critical issue that affects the measured nanomechanical response.[15] Usually, researches limit localized deformations (indentations) to depths much smaller than the total thickness of the films (< 20%) to eliminate the influence of the solid support.[15] In our case, the trigger set point of 3 nm is much less than 1% of the film thickness (10 μm). Thus, the decreased modulus for the PS blocks and increased modulus for the PEB's mainly results from the microstructure change that is governed by the volume ratio of the phases. At low volume fraction of PS, the soft PEB blocks surround and support the PS blocks underneath, while at high volume fraction of PS, the microstructure changes to be more PS phase dominated. It should be noticed that the Young's modulus reported by Tsukruk et al.[15] are 20 ± 7 MPa for the glassy domains PS and 7 ± 3 MPa for the rubber phase PEB of a molecularly thick SEBS layers; those reported by Motomatsu et al.[24] are 24 ± 3.1 MPa for the PS and 6.4 ± 0.3 MPa for the PEB of a SEBS (15/70/15) sample. The variation of determined Young's modulus may result from the AFM measurement, such as tip radius, tip geometry, and different contact model.[24,35] Other possibilities include sample preparation such as film thickness.

As mentioned above, the JKR analysis fits well for the elastic PS component but deviations appear for the viscoelastic PEB component because of the viscoelastic effect. The deviated work as indicated by the shaded region in Figure 4a is obtained simultaneously. Here we demonstrate that a map of deviated work of SEBS (14.5/71/14.5) can differentiate viscoelasticity between the PS and PEB component (Figure 5). It indicates that the map of deviated work can also clearly differentiate the two chemical blocks of the copolymer. However, the deviated work contrast between the hard PS and soft PEB blocks is inverted in comparison to the Young's modulus map. The softer PEB blocks show higher deviated work than the hard PS blocks. Thus, the deviation mapping from elastic model will be a convenient technique to visualize the distribution of viscoelasticity.

Besides nanomechanical properties, we can also obtain the deformation image and true surface morphology of the block copolymers simultaneously with the nanomechanical mapping technique. It is well-known that the height images obtained from tapping mode and FV are affected by the sample deformation caused by the force between the probe tip and the sample.[29,34,35] Such images are usually misinterpreted as topographies. This happens more frequently when the sample is soft materials such as polymeric or biorelated materials. However, here we will show the true height images obtained using the nanomechanical mapping technique. Figure 6 shows the generated original height, sample deformation, and reconstructed true height images. The original height image (Figure 6a) is calculated from the set of Piezo displacement at a constant trigger force. It contains artifacts due to the deformation caused by the low elastic modulus of the rubbery PEB component. The true height image (Figure 6c) can be considered as the superimposition of the original height image and the sample deformation image. The weak contrast of the true height image is due to large compensation of the deformation at the soft PEB regions. As can be seen from Figure 6c, the reconstructed height image indicates that the sample surface is essentially flat with a surface roughness less than 4 nm. It is worthy to mention that similar conclusion has also

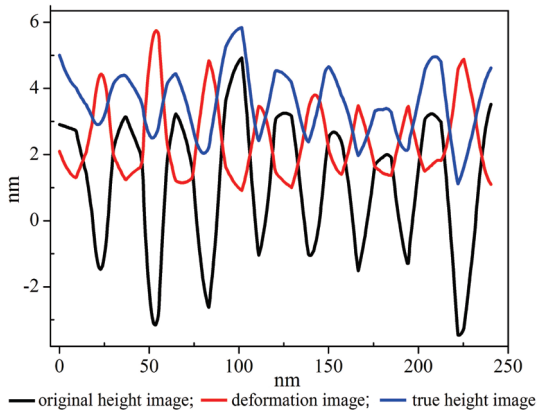

Figure 7. Section analysis of the original height, deformation, and true height image.

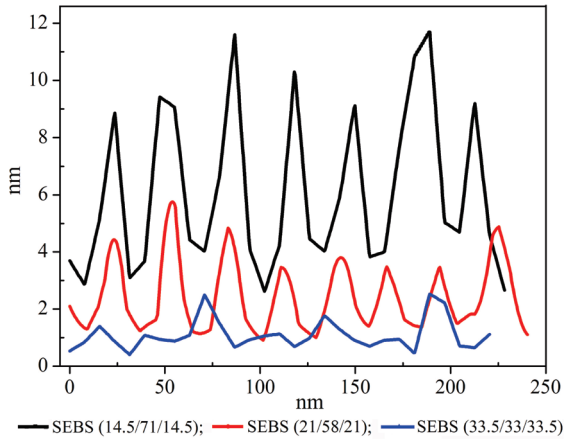

Figure 8. Section analysis of the deformation images of the SEBS samples having different component weight ratio.

been reported by Krausch et al., who use a 30 × 30 array of amplitude/phase vs distance (APD) curves obtained with AFM to reconstruct the "real" surface of poly(styrene-*block*-butadiene-*block*-styrene) (SBS) model system.[36] By comparing the section analysis of the original height, deformation, and true height images (Figure 7), it is found that the height value is greatly decreased. The decrease in height values is due to the large deformation caused by the force between the probe tip and the sample. However, the reconstructed true height image reveals the true surface topography free from sample deformation.

Figure 8 shows a section analysis on the deformation image of the SEBS samples having different PS weight ratio. At low PS component (SEBS(14.5/71/14/5)), the deformation caused by tapping force is about 10 nm. As the PS weight ratio further increases, the deformation caused by the same tapping force gradually decreases. Such a result is consistent with the above conclusion that both the Young's modulii and the deformations strongly depend on the microstructure which is dominated by composition.

4. Conclusions

In conclusion, we have investigated the effect of composition on the surface morphology and nanomechanical properties of SEBS using a nanomechanical mapping technique developed in our group. The true topography, elastic modulus, and deviated work together with the original height and deformation images have been obtained simultaneously in a force mapping. The calculated local Young's modulii for both PS and PEB blocks strongly depends on the microstructure whose formation is affected predominantly by composition. As the PS weight ratio increases, the modulus of PS blocks increase from 19.2 ± 2.5 MPa for SEBS (10/80/10) to 823.0 ± 168.1 MPa for SEBS (33.5/33/33.5), while PEB's increases from 8.7 ± 2.1 MPa for SEBS (10/80/10) to 97.6 ± 17.8 MPa for SEBS (33.5/33/33.5). The original topography directly obtained from the force volume mode is demonstrated to be an artifact because of the deformation caused by the tapping force. However, the reconstructed true height image reveals the true topographic feature free from sample deformation. The result of deviation mapping from elastic model provides a convenient way to visualize the distribution of viscoelasticity.

Acknowledgment. The authors thank Dr. Kazuya Nagata of the Asahi Kasei Chemicals Corp. for technical assistance. This work was supported by the Grant-in-Aid for Scientific Research (B) (21350120) from the Japan Society for the Promotion of Science.

References and Notes

(1) Bates, F. S.; Fredrickson, G. H. Block copolymer thermodynamics: theory and experiment. In *Thermoplastic elastomers*, 2nd ed.; Holden, G., Legge, N. R., Quirk, R. P., Schroeder, H. E., Eds.; Hanser: Munich, Germany, 1998; pp 336−364.
(2) Holden, G. *Understanding thermoplastic elastomers*. Hanser: Munich, Germany, 2000; pp 15−35.
(3) Adhikari, R.; Michler, G. H. *Prog. Polym. Sci.* **2004**, *29*, 949–986.
(4) Lynd, N. A.; Meuler, A. J.; Hillmyer, M. A. *Prog. Polym. Sci.* **2008**, *33*, 875–893.
(5) Michler, G. H. *Trends Polym. Sci.* **1995**, *3*, 124–131.
(6) Wang, D.; Fujinami, S.; Nakajima, K.; Nishi, T. *Macromolecules* **2010**, *43*, 3169–3172.
(7) Sahin, O.; Magonov, S.; Su, C. M.; Quate, C. F.; Solgaard, O. *Nat. Nanotechnol.* **2007**, *2*, 507–514.
(8) Sahin, O.; Erina, N. *Nanotechnology* **2008**, *19*, 445717.
(9) Jesse, S.; Kalinin, S. V.; Proksch, R.; Baddorf, A. P.; Rodriguez, B. J. *Nanotechnology* **2007**, *18*, 435503.
(10) Stan, G.; Cook, R. F. *Nanotechnology* **2008**, *19*, 235701.
(11) Stan, G.; Ciobanu, C. V.; Parthangal, P. M.; Cook, R. F. *Nano Lett.* **2007**, *7*, 3691–3697.
(12) Wang, D.; Fujinami, S.; Nakajima, K.; Inukai, S.; Ueki, H.; Magario, A.; Noguchi, T.; Endo, M.; Nishi, T. *Polymer* **2010**, *51*, 2455–2459.
(13) Nishi, T.; Nukaga, H.; Fujinami, S.; Nakajima, K. *Chin. J. Polym. Sci.* **2007**, *25*, 35–41.
(14) Nagai, S.; Fujinami, S.; Nakajima, K.; Nishi, T. *Compos. Interface* **2009**, *16*, 13–25.
(15) Tsukruk, V. V.; Sidorenko, A.; Gorbunov, V. V.; Chizhik, S. A. *Langmuir* **2001**, *17*, 6715–6719.
(16) Tsukruk, V. V.; Sidorenko, A.; Yang, H. *Polymer* **2002**, *43*, 1695–1699.
(17) Kluge, D.; Abraham, F.; Schmidt, S.; Schmidt, H. W.; Fery, A. *Langmuir* **2010**, *26*, 3020–3023.
(18) Ganguly, A.; Sarkar, M. D.; Bhowmick, A. K. *J. Polym. Sci., Part B: Polym. Phys.* **2007**, *45*, 52–66.
(19) Ganguly, A.; Bhowmick, A. K. *J. Appl. Polym. Sci.* **2009**, *111*, 2104–2115.
(20) Johnson, K. L.; Kendall, K.; Roberts, A. D. *Proc. R. Soc. London, Ser. A* **1971**, *324*, 301–313.
(21) Sun, Y.; Walker, G. C. *Langmuir* **2004**, *20*, 5837–5845.
(22) Ho, R. M.; Adedeji, A.; Giles, D. W.; Hajduk, D. A.; Macosko, C. W.; Bates, F. S. *J. Polym. Sci., Part B: Polym. Phys.* **1997**, *35*, 2857–2877.
(23) Han, X.; Hu, J.; Liu, H. L.; Hu, Y. *Langmuir* **2006**, *22*, 3428–3433.
(24) Motomatsu, M.; Mizutani, W.; Tokumoto, H. *Polymer* **1997**, *38*, 1779–1785.
(25) Ganguly, A.; Bhowmick, A. K. *Macromolecules* **2008**, *41*, 6246–6253.
(26) Wang, L.; Hong, S.; Hu, H. Q.; Zhao, J.; Han, C. C. *Langmuir* **2007**, *23*, 2304–2307.
(27) McLean, R. S.; Sauer, B. B. *Macromolecules* **1997**, *30*, 8314–8317.
(28) Raghavan, D.; Gu, X.; Nguyen, T.; VanLandingham, M. R.; Karim, A. *Macromolecules* **2000**, *33*, 2573–2583.

(29) Bar, G.; Thomann, Y.; Brandsch, R.; Cantow, H. J.; Whangho, M. H. *Langmuir* **1997**, *13*, 3807–3812.
(30) Bar, G.; Thomann, Y.; Brandsch, R.; Whangbo, M. H. *Langmuir* **1998**, *14*, 1219–1226.
(31) Sauer, B. B.; McLean, R. S.; Thomas, R. R. *Langmuir* **1998**, *14*, 3045–3051.
(32) Magonov, S. N.; Elings, V.; Papkov, V. S. *Polymer* **1997**, *38*, 297–307.
(33) VanLandingham, M. R.; Eduljee, R. F.; Gillespie, J. W. *J. Appl. Polym. Sci.* **1999**, *71*, 699–712.
(34) Magonov, S. N.; Ellings, V.; Whangbo, M. H. *Surf. Sci.* **1997**, *375*, L385–L391.
(35) Kopycinska-Müller, M.; Geiss, R. H.; Hurley, D. C. *Ultramicroscopy* **2006**, *106*, 466–474.
(36) Knoll, A.; Magerle, R.; Krausch, G. *Macromolecules* **2001**, *34*, 4159–4165.